Finite-Element Parametric Study of the Consolidation Behavior of a Trial Embankment on Soft Clay

Wenxiong Huang[1]; Stephen Fityus[2]; Daniel Bishop[3]; David Smith[4]; and Daichao Sheng[5]

Abstract: The paper presents a case study for numerical analysis of the consolidation behavior of an instrumented trial embankment constructed on a soft soil foundation. Details are given to the geological profile, field instrumentation, laboratory test results, and determination of soil parameters for numerical modeling. Embankment settlement is estimated based on one-dimensional consolidation analysis and nonlinear finite-element analysis following Biot's consolidation theory. Finite-element results are calibrated against the measured field data for a period of more than 3 years. Development and dissipation of excess pore pressure, long-term settlement, and horizontal displacement are predicted and discussed in light of sensitivity of embankment performance to some critical factors through a parametric study.

DOI: 10.1061/(ASCE)1532-3641(2006)6:5(328)

CE Database subject headings: Finite element method; Soil consolidation; Embankment; Soft soils; Clays; Foundations.

Introduction

As part of a program to upgrade the Pacific Highway (located in the coastal regions of Eastern Australia), the "Ballina Bypass" is to be constructed by the Roads and Traffic Authority (RTA) of New South Wales. A large proportion of the bypass is to be constructed on soft clay soil that is widespread in the Ballina area. In order to assess the likely foundation behavior, two trial embankments were constructed during 1998. They were instrumented with settlement plates, vertical settlement profilers, vibrating wire piezometers, and horizontal profilers. Site investigation, sampling, laboratory tests and installation of instruments were performed by the RTA and Robert Carr & Associates, Australia. Using the data that have been collected for a period of more than 3 years, a systematic analysis has now been performed to better understand the embankment behavior and for reference of the geotechnical design.

[1]ARC APD Fellow, School of Engineering, Univ. of Newcastle, Callaghan, NSW 2308, Australia. E-mail: wenxiong.huang@newcastle.edu.au

[2]Senior Lecturer, School of Engineering, Univ. of Newcastle, Callaghan, NSW 2308, Australia. E-mail: stephen.fityus@newcastle.edu.au

[3]Ph.D. Student, School of Engineering, Univ. of Newcastle, Callaghan, NSW 2308, Australia. E-mail: daniel.bishop@studentmail.newcastle.edu.au

[4]Professor, Dept. of Civil and Environmental Engineering, Univ. of Melbourne, VIC 3010, Australia. E-mail: david.smith@civenv.unimelb.edu.au

[5]Senior Lecturer, School of Engineering, Univ. of Newcastle, Callaghan, NSW 2308, Australia. E-mail: daichao.sheng@newcastle.edu.au

Note. Discussion open until March 1, 2007. Separate discussions must be submitted for individual papers. To extend the closing date by one month, a written request must be filed with the ASCE Managing Editor. The manuscript for this paper was submitted for review and possible publication on May 18, 2004; approved on July 18, 2005. This paper is part of the ***International Journal of Geomechanics***, Vol. 6, No. 5, October 1, 2006. ©ASCE, ISSN 1532-3641/2006/5-328–341/$25.00.

This paper presents a numerical analysis of the "Teven Road trial embankment," based on the field data and results from laboratory tests. For this purpose, a geotechnical model is established based on the borehole logs in conjunction with cone penetration test (CPT) data. Soil parameters for the numerical analysis have been estimated on the basis of laboratory test results. The work is aimed at providing a complete case study by comparing conventional settlement analysis and finite-element analysis with field monitoring data from the instrumented embankment. Much effort is put toward how to achieve reliable results based on obtained laboratory and field data. Due to the nature of site investigation, soil sampling, and soil tests, some inaccuracies exist inevitably in both the monitored data and estimated soil parameters. In particular, early stage soil sampling at the Teven Road site was focused on the soft clay layer over the sand layer and missed the sand layer. Assumed values are used for soil parameters in this layer for numerical analysis. In order to cope with these uncertainties and to study the influence of some critical parameters for a better assessment of embankment behavior, parametric studies have been performed in the numerical analysis.

Finite-element calculations are performed with the commercial finite-element program ABAQUS (HKS 2001). The consolidation process of the embankment foundation is modeled as a quasistatic deformation problem of porous media coupled to pore–water flow following Biot's theory (Biot 1941). The dissipation of developed excess pore pressure due to loading is governed by Darcy's law. The soft clay under the embankment is modeled with the well-established Modified Cam Clay (MCC) model (Roscoe and Burland 1968). The model has an important advantage in that the main aspects of soil behavior are captured with only a few material parameters, which are well defined and easy to determine. For further analysis, more advanced and sophisticated constitutive models, such as HiSS models developed by Desai and his coworkers (e.g., Wathugala and Desai 1993; see, also, Desai 2000) and the MIT-E3 model (Whittle and Kavvadas 1994), may be used. A stiff sand layer is sandwiched horizontally in the soft clay at a depth of about 8–11 m, which is modeled with the Drucker–Prager elastic–perfect-plastic model in the finite-element analysis. We note that the shear-dilatation behavior of sands is better mod-

eled with more advanced constitutive models, for instance, a HiSS model (Desai 2000) or a hypoplastic model (Gudehus 1996). The employment of this simple model is mainly due to the lack of test data for this soil layer. It can also be noted that as this thin sand layer constitutes a horizontal drainage channel in the soft clay, its contribution to embankment settlement due to deformation is, compared with the contributions from the soft clays over and beneath it, negligible.

Bjerrum (1967) suggested that soil deformation is composed of instant deformation and delayed deformation. The instant deformation develops simultaneously with the increase of effective stress causing a reduction in void ratio. It becomes time dependent only due to the fact that time is needed for excess pore pressure in soil to dissipate and for the load to be transferred to the soil skeleton. The delayed compression represents the reduction in soil volume due to the rheological (creep) effect. It often becomes more apparent after the excess pore pressure is substantially dissipated, even though it occurs at the very beginning of deformation. The continuing deformation in soil under constant effective stress, which is conventionally referred to as the "secondary" consolidation, usually constitutes only a small fraction in the total consolidation deformation. In contrast, the "primary" consolidation, which is the combination of Bjerrum's instant compression and delayed compression over the time period of pore pressure dissipation, constitutes the major part of the total consolidation deformation. With the present time-independent constitutive model in numerical analysis, the time-dependent creep deformation is not taken into account. The predicted final settlements described here can be considered to be primary or the consolidation settlement due to instant deformation. Neglecting creep effect is assumed to have only an insignificant influence on the numerical results as the soil parameters are determined based on the tests without distinguishing instant and delayed deformation.

Site Conditions and Soil Properties

The Teven Road embankment is located adjacent to the existing Pacific Highway, 2 km south of the town of Ballina in northern New South Wales, Australia. The town and much of the proposed bypass are situated on a flood plain overlying an infilled quaternary estuary near the mouth of the Richmond River. The embankment is 0.2 km from Emigrant Creek (a tributary of the Richmond River), 1 km from the Richmond River, and 7 km from the river mouth.

Detailed subsurface investigation was undertaken by Robert Carr & Associates (2000). Based on the drilled bore logs and CPT, the soil foundation can roughly be stratified into four layers, as shown in Fig. 1(a). On top is a thin layer of desiccated clay, forming a crust about 1 m thick, which is slightly sandy, usually unsaturated, and overconsolidated. The cone tip resistance (q_t) values are around 700 kPa and s_u values are between 75 and 100 kPa. Beneath the crust is a thick, estuarine clay deposit to a depth of about 30 m. The clay has extremely high moisture content, up to around 130%. Undrained shear strength ranges from 16 to 33 kPa while the cone tip resistance is around 200–300 kPa. This clay deposit is divided into two layers by a sand layer, lying almost horizontally between average depths of 8.5 and 11.5 m. This layer of dense, fine- to medium-grained sand is indurated and somewhat cemented. CPT tests were unable to penetrate it in many locations due to bending of the cone rod. However, pumping tests have shown that this unit is still porous with a relatively high permeability over its thickness, and so is considered to form a horizontal drainage channel within the clay deposit. The clay layer above the sand layer is soft, while the clay layer under the sand layer gradually varies from soft to firm to stiff with increasing depth. Beneath this clay layer is a stiff residual soil or bedrock, whose deformation is neglected in the analysis. A detailed discussion of the geomorphology of the quaternary sediment sequence is presented by Bishop (2004).

For numerical analysis, soil parameters are estimated based on careful sampling and laboratory testing, or on correlations with field test data. For the Teven Road trial embankment, undisturbed soil samples have been taken from the soft clay layers and tested. The main results from laboratory tests are listed in Table 1. The initial void ratio e_o, soil dry density ρ_d, the plasticity index I_p, and the liquidity index I_L, are obtained from soil characterization tests, while the overconsolidation ratio $OCR=\sigma'_{v\,max}/\sigma'_v$, the coefficient of volume change m_v, the coefficient of consolidation c_v, the compression index C_c, the recompression index C_r, and the secondary compression index C_α, are obtained from one-dimensional (1D) consolidation tests. The friction angle ϕ' is obtained from drained triaxial compression tests.

Instrumentation

The base of the trial embankment is 84 m long and 54 m wide. It was lifted to a total fill thickness of 1.6 m over a period of 69 days. The general construction sequence for the trial embankment consisted of mowing the vegetation, laying a geofabric layer over the entire embankment footprint, positioning settlement plates, placing a 0.75 m bridging layer of "crusher dust" and a 0.25 m layer of free-draining aggregate, installing instrumentation, placing a geofabric layer over the aggregate, and finally, constructing the embankment from gravelly clay fill. Location of the instrumentation is shown in Fig. 1(b).

Measured data include settlements from settlement plates, readings of pore pressure from piezometers, and horizontal displacement profiles from inclinometers. These data describe the fundamental responses of an embankment on soft soil and they are essential for the calibration of analytical models to predict embankment behavior.

However, it is important to note that although the Teven Road embankment project was set up to collect all of the data needed to calibrate a numerical model for embankment behavior, the available measured data are incomplete. For example, pore pressure data are only available corresponding to embankment heights greater than 0.5 m, as piezometers were not installed until after a 0.5 m working platform had been constructed. Furthermore, although vertical settlement profilers were installed, due to a problem, no data for the settlement in the different soil layers were obtained. Also, the first reading of the inclinometers was not taken until 42 days after the start of construction (which does not include the early horizontal movements), so that these data can only be used to assess predictions of lateral displacements that might occur relative to the conditions in the soil mass that prevailed at a time of 42 days after construction.

Estimation of Embankment Settlement Based on 1D Consolidation Tests

In engineering practice, foundation settlement is usually estimated empirically based on one-dimensional consolidation tests.

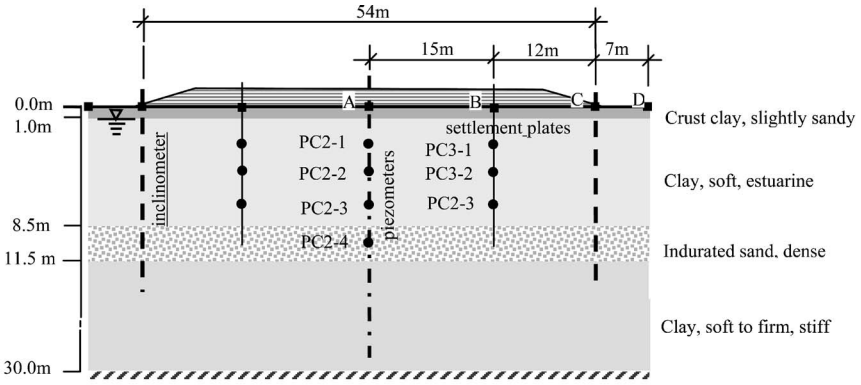

(a) geotechnical model of a section across Teven Road trial embankment (section at line M)

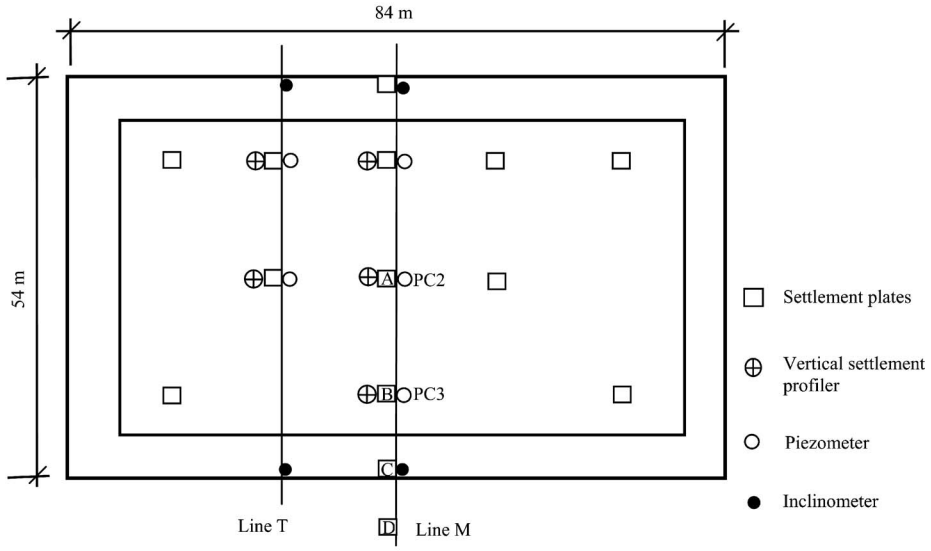

(b) plan view of the Teven Road trial embankment showing instrumentation locations.

Fig. 1. Details of the Teven Road trial embankment

Such results are included here as a reference for comparison with the results from the following numerical analysis. The total settlement s_t of a foundation is computed as the sum of an immediate settlement s_i, which is elastic under undrained conditions, and a subsequent consolidation settlement s_c (i.e., $s_t=s_i+s_c$). The immediate settlement of the foundation can be estimated from the results of elasticity theory using the influence factor method for a trapezoidal embankment (e.g., Das 1990), which produces a result of $s_i \approx 35$ mm for the considered embankment with an average value of the undrained elastic modulus of $E_u=6{,}000$ kPa for the Ballina clay.

The time-dependent consolidation settlement s_c takes place as a result of the extrusion of pore water from the void space and reorganization of soil structure. It is a conventional approach to divide the consolidation into primary and secondary phases. The primary settlement s_p is the soil deformation observed during the

Table 1. Engineering Properties and Initial Parameter Values for the Teven Road Soil Profile

Depth (m)	e_0	σ_{v0} (kPa)	OCR	I_p	I_L	m_v ($\times 10^{-4}$ m^2/kN)	c_v (m^2/year)	C_c	C_r	C_α^*	ϕ' (degrees)
0.7	0.80	6	8.0	0.40	0.63	12.20	185.65	0.18	0.025	0.002	33
1.7	1.25	11	5.3	0.36	0.92	12.78	14.844	0.51	0.03	0.012	—
2.7	2.01	16	2.44	0.58	0.98	9.84	3.001	1.09	0.07	0.032	26
3.7	2.27	21	1.71	0.71	0.81	8.22	4.654	1.11	0.05	0.025	—
4.8	2.82	26	1.92	0.81	1.04	6.63	2.255	1.94	0.05	0.050	28
6.7	2.70	33	1.51	0.77	1.01	5.09	5.832	1.43	0.04	0.044	—
14.7	1.69	62	1.06	0.38	1.07	3.06	7.161	0.31	0.02	0.005	28

Note: C_α^* has been interpreted from the 100 kPa load increment.

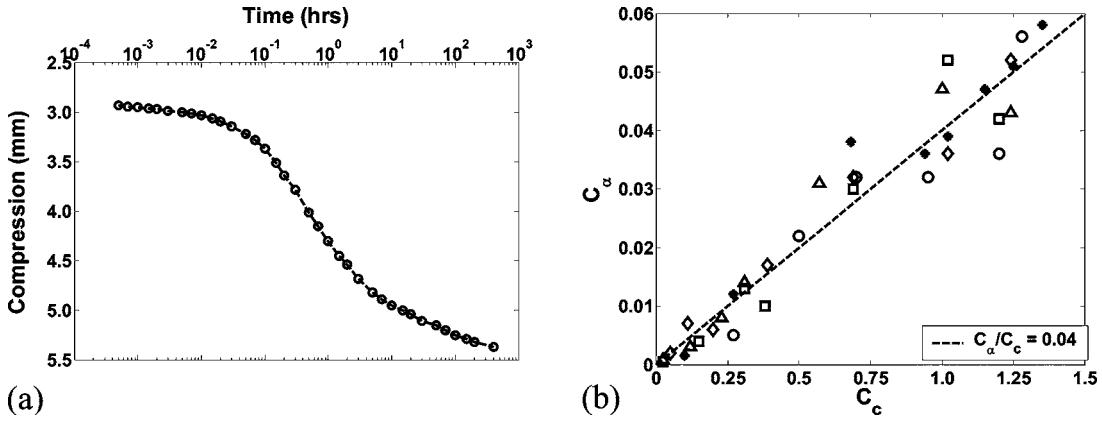

Fig. 2. (a) Compression–time curve; (b) C_α/C_c relation from laboratory tests

dissipation of excess pore pressure, which usually constitutes the major part of the total consolidation settlement, and the secondary settlement s_s is the continuing deformation of soil under constant effective stress, after the excess pore pressure is substantially dissipated.

Primary Consolidation Settlement

The primary consolidation settlement can be directly estimated based on the results from the standard 1D consolidation test. Subdivision of soil profile into layers is often necessary to cope with the variation of the effective stress and soil compressibility with depth. Thus, $s_p=\Sigma_i s_{pi}$, where s_{pi} is computed for each sublayer of soil using a strain hardening soil model

$$s_{pi}=\frac{C_r\Delta z_i}{1+e_o}\log_{10}\left(\frac{\sigma'_{vo}+\Delta\sigma'_{vi}}{\sigma'_{vo}}\right) \quad \text{for } \sigma'_{vo}+\Delta\sigma'_{vi}<\sigma'_{po} \quad (1a)$$

$$s_{pi}=\frac{C_r\Delta z_i}{1+e_o}\log_{10}\left(\frac{\sigma'_{po}}{\sigma'_{vo}}\right)+\frac{C_c\Delta z_i}{1+e_o}\log_{10}\left(\frac{\sigma'_{vo}+\Delta\sigma'_{vi}}{\sigma'_{po}}\right)$$
$$\text{for } \sigma'_{vo}<\sigma'_{po}<\sigma'_{vo}+\Delta\sigma'_{vi} \quad (1b)$$

Herein, σ'_{vo}=initial vertical stress; $\Delta\sigma'_{vi}$=effective vertical stress increment due to the embankment; σ'_{po} represents preconsolidation stress; and Δz_i denotes the thickness of sublayers with a total thickness $H=\Sigma_i\Delta z_i$. The increase of vertical stress under the embankment can be estimated using elastic theory (see, for instance, Poulos and Davis 1974). With the obtained stress increment, Eq. (13) produces a primary consolidation settlement of s_p=423 mm, in which the contribution from compression of the lower clay layer (Layer 4) is about 147 mm. The contribution from compression of the indurated sand layer is neglected as it is much stiffer than the clay layers.

Secondary Consolidation and Long-Term Settlement

Many laboratory data show that, within a limited time span, the secondary compression in soils increases more or less linearly with the logarithm of time, which is also the case for Ballina clay, as shown in Fig. 2(a). In the laboratory, the rate of the secondary consolidation is expressed by the secondary compression index

$$C_\alpha=\frac{\Delta e}{\Delta\log_{10}t} \quad (2)$$

Mesri and Godlewski (1977) suggested that the compression index be linearly related to the secondary compression index, and the value of C_α/C_c fall in a narrow range of 0.02–0.10 for a variety of natural soils. They found that C_α/C_c has a typical value of 0.04±0.01 for an inorganic soft clay. This is roughly true for the Ballina clay [Fig. 2(b)].

As long as the secondary compression index remains constant, the secondary compression of soil may be estimated according to

$$s_s=\frac{C^*_\alpha}{1+e_{100}}h\log_{10}(t/t_p) \quad \text{for } t<t_p \quad (3)$$

where t_p represents the end-of-primary consolidation time and h stands for the thickness of the soil sample.

Prediction of the long-term settlement with secondary consolidation has long been a difficult task (Olson 1986). The current data for the Teven Road trial embankment are not sufficient to allow a reliable assessment in this case. Difficulties arise in using Eq. (3) for the prediction of secondary compression in the field situation, as this equation is valid only for a limited time. Beyond this time limit, the rate of secondary compression may decrease gradually or rapidly to zero (see, for instance, Lo et al. 1976). In laboratory tests, this time can be a few weeks. On the other hand, there are no field data to indicate that the secondary slopes measured 24 h or 2 weeks in the laboratory can be used to reliably predict field behavior over a period of decades.

In cases where Eq. (3) is used to describe secondary compression in the field, the end-of-primary time t_p has a strong influence on the results. In a thick, soft clay layer, due to the large drainage distance involved, the primary consolidation can be so retarded that, in extreme cases, all of the secondary compression has been completed first. Most often, the completion of the primary consolidation often requires several decades, the time for which the secondary compression ceases is generally less than 10 times of t_p (Mesri and Choi 1985). Taking the present trial embankment as an example, the field end-of-primary consolidation time from finite-element analysis is about $t_p\approx 20$ years for the upper clay layer and $t_p>50$ years for the lower clay layer. If the secondary compression can last for 100 years, Eq. (3) yields an estimation of $s_s\approx 60$ mm for the secondary consolidation settlement.

Estimation of Soil Parameters for Finite-Element Analysis

The MCC model has been used to model clayey soil behavior. The details regarding the model and its finite-element implementation can be found elsewhere (e.g., Wood 1990; Gens and Potts 1988). The original critical state of the model was formulated based on conventional triaxial tests. In this numerical analysis, a generalization to take into account the variation of the limit stress ratio in the deviatoric stress plane is accepted by using the following modified yield condition:

$$f = \left(\frac{p'}{p_0} - 1\right)^2 + \left(\frac{\tilde{q}}{Mp_0}\right)^2 - 1 = 0 \tag{4}$$

where p' denotes the mean effective pressure; and $\tilde{q} = (1/2)q[1 + 1/\beta - (1 - 1/\beta)(J_3/q)^3]$ = generalized deviatoric stress with $J_3 = [(9/2)s_{ij}s_{jk}s_{ki}]^{1/3}$ being the third stress invariant. β = parameter to control the shape of the yield surface in the deviatoric stress plane, which can be set to 0.8 in most calculations (HKS 2001). The model includes the consolidation parameters (λ and κ), the drained strength parameter (ϕ' or M), and the elastic parameter (μ' or G'). The consolidation parameters λ and κ represent the gradient of the normal compression line and the gradient of the unloading/reloading line in the $\ln p' - v$ plane, respectively ($v = 1 + e$ is the specific volume). They can be related to the compression index C_c and the recompression index C_r by

$$\lambda = C_c/\ln 10, \quad \kappa = C_r/\ln 10 \tag{5}$$

The shear strength parameter M is related to the critical friction angle, ϕ', according to

$$M = 6 \sin \phi'/(3 - \sin \phi') \tag{6}$$

A constant Poisson's ratio μ' is assumed in this study. The elastic behavior is governed by two parameters κ and μ', by which the bulk modulus K' and the shear modulus G' are determined

$$K' = \frac{vp'}{\kappa}, \quad G' = \frac{3(1 - 2\mu')K'}{2(1 + \mu')} \tag{7}$$

Clays have a typical Poisson's ratio value around 0.3, varying slightly with respect to the soil plasticity index I_p (Wroth 1975).

Hardening/softening behavior is controlled by a state parameter p_0', which is related to the plastic volumetric strain, $d\varepsilon_v^p$, by

$$\frac{dp_0'}{p_0'} = \frac{v}{\lambda - \kappa} d\varepsilon_v^p \tag{8}$$

The initial state can significantly affect the predicted soil response and, therefore, it needs to be defined carefully. In the embankment foundation, the initial vertical effective stress distribution can be obtained simply and reliably from measured values of soil unit weight, and the initial horizontal stress can be defined with the earth pressure coefficient at rest K_0. For the normally consolidated (nc) soil, K_0 can be related to the friction angle by Jâky's estimation

$$K_{0nc} = (1 - \sin \phi') \tag{9}$$

For overconsolidated clay, the following relation is considered to give a fairly good estimation for K_0 (Wood 1990)

$$K_0 = K_{0nc}\sqrt{\text{OCR}} \tag{10}$$

The initial yield surface can be defined with respect to the initial stress state. To this end, a mean effective stress ratio $n_p = p'_{max}/p'$ is introduced with p'_{max} representing the maximum mean pressure reached in the history. n_p is then related to the ratio OCR by

$$\frac{n_p}{\text{OCR}} = \frac{1 + 2K_{0nc}}{1 + 2K_0} \tag{11}$$

The initial yield surface can be determined by p_0' from

$$\frac{p_0'}{p'_{max}} = 1 + \frac{\eta_{Knc}^2}{M^2} \quad \text{with } \eta_{Knc} = 3(1 - K_{0nc})/(1 + 2K_{0nc}) \tag{12}$$

A simple Drucker-Prager–elastoplastic model is adopted to describe the sand layer and the embankment fill. The soil response is basically elastic governed by two parameters E' and μ' with the former related to κ through $E' = 3(1 - 2\mu')vp'/\kappa$. Plastic flow occurs when the shear strength limit is reached

$$f = q - p' \tan \beta' - d' = 0 \tag{13}$$

Two Drucker–Prager parameters β' and d' can be related to the widely used Mohr–Coulomb shear strength parameters ϕ' and c'. For plane strain problems with an associated flow rule, these relations are

$$\tan \beta' = \frac{\sqrt{3} \sin \phi'}{\sqrt{1 + \frac{1}{3} \sin^2 \phi'}}, \quad \frac{d'}{c'} = \frac{\sqrt{3} \cos \phi'}{\sqrt{1 + \frac{1}{3} \sin^2 \phi'}} \tag{14}$$

The permeability or hydraulic conductivity in the vertical direction for the subsoil layers, k_v, has been estimated mainly from 1D consolidation tests. As some of the values of the permeability obtained in this way are rather scattered, direct permeability tests have been conducted using the falling head test with the undisturbed samples taken at a depth of 7.5 m. Some CPTu dissipation test data have also been collected for an indirect estimation of horizontal permeability (Lunne et al. 1997). These tests verified the order of correctness of the values of permeability listed in Table 2 for Soil Layer 2.

Natural clayey soils often show higher permeability in the horizontal direction than in the vertical direction. According to Al-Tabbaa and Wood (1987), the permeability anisotropy ratio $r_k = k_h/k_v$ for clayey soils may vary from 1.0 to 3.0, and can be related to the liquidity index I_L. In the heavily overconsolidated London clay, Chandler et al. (1990) found r_k values having an average of about 2. Leroueil et al. (1990), however, found that in marine clays, r_k can be as low as 1.0 to 1.2, and the permeability anisotropy does not vary significantly for strains up to 25%. In the present numerical analysis, a permeability anisotropy ratio of $r_k = 2.0$ is assumed in most calculations.

Due to inadequate in situ testing and sampling, there are no available laboratory data for the sand layer. Therefore, all model parameters adopted for this layer are assumed values. In the four parameters in the Drucker–Prager model, typical values can be adopted for the Poisson's ratio μ' with good confidence, and the shear strength parameters ϕ' and c' can be estimated with reasonable certainty. The elastic modulus E' is related to parameter κ. As κ values in sand may vary over a relatively wide range, sensitivity to its variation is assessed by comparing the results of numerical tests performed for different values.

Calibration of MCC parameters was made by a back analysis, that is, by matching the model response with the laboratory test

Table 2. Best Estimate (Default) Values Used in the Standard Numerical Analyses

Soil layer	Depth (m)	e_0	γ_t (kN/m^3)	OCR	K_0	MCC parameters					k_v (m/s)
						κ	μ'	λ	e_{cs}	M	
1	0–1.0	0.80	18.94	8	1.28	0.011	0.3	0.078	0.98	1.33	7.0×10^{-8}
2	1.0–2.5	2.29	15.08	5.3	1.10	0.020	0.33	0.587	3.94	1.07	1.65×10^{-9}
	2.5–3.5			2.4	0.84						
	3.5–8.5			1.6	0.65						
3	8.5–11.5	0.65	19.80	—	0.56	$\kappa=0.004$, $\mu'=0.28$, $\phi'=30°$, $c'=5.0$ kPa					1.0×10^{-6}
4	11.5–15	1.69	15.99	1.06	0.54	0.009	0.3	0.134	2.18	1.11	6.95×10^{-10}
	15.0–20.0			1.03	0.52						
	20.0–30.0			1.00	0.50						
Fill			18.0			$E'=5000$ kPa, $\mu'=0.30$, $\phi'=28°$, $c'=10.0$ kPa					

results. In summary, the best-estimate values of the soil parameters, for the four soil layers in the geotechnical model, are listed in Table 2. An averaging procedure with respect to thickness of subsoil layers has been used to obtain the values for the second soil layer. As mentioned above, some soil parameters are sensitive to the change of environment during sampling, and may have quite different values under in situ conditions. In addition, there is considerable measurement uncertainty due to the inherent variability of the soil deposit. The effects of such uncertainty are investigated by means of the following parametric study, in which one parameter is varied while the rest take the best-estimate values given in the table below.

Numerical Details

In the present finite-element analysis, the problem is solved as a two-dimensional (2D) plane strain consolidation problem with a symmetry condition applied at the centerline of the embankment. A computation domain of 30 m vertically by 94 m horizontally (from the axis of symmetry) is discretized into 390 elements, as shown in Fig. 3. The width of the area selected for the numerical modeling is large enough (more than three times the embankment width), so that the boundary at the right side will have a negligible influence on the results.

The boundary conditions prescribed are as follows. On the left-hand side (the axis of symmetry in Fig. 3), horizontal displacements and water fluxes are zero, so that the symmetry condition is achieved. The bottom boundary is ascribed conditions of zero displacement and imperviousness. On the right-hand side, while displacement is fixed, the pore water is allowed to flow across the boundary, so that the possible horizontal water flow condition is not affected significantly using a finite domain. At the ground surface, conditions of free drainage and unconstrained displacement apply. Numerical calculations were performed to model the actual construction sequence for the embankment, which was raised up to a thickness of 1.60 m in 69 days, as shown in Fig. 4. For convenience of presentation, the data are presented in terms of the time (days) from a reference time of day zero on September 4, 1998. Long-term consolidation is estimated by continuing the computation until the excess pore pressures in soil layers are substantially dissipated.

Basic Features of Embankment Behavior and the Effect of Soil Permeability

Ground settlement has been measured at the following points along a transverse section line *M* (refer to Fig. 1): (A) in the center of the embankment; (B) 15 m from the center; (C) at the toe of the embankment (27 m from the center); and (D) 7 m outside the embankment (34 m from the center).

Pore pressures were measured with Piezometer PC2 (refer to Fig. 1) at Point PC2-1 (3 m deep), Point PC2-2 (5 m deep), Point PC2-3 (7 m deep), and Point PC2-4 (10 m deep) and with piezometer PC3 (refer to Fig. 1) at Point PC3-1 (3 m deep), Point

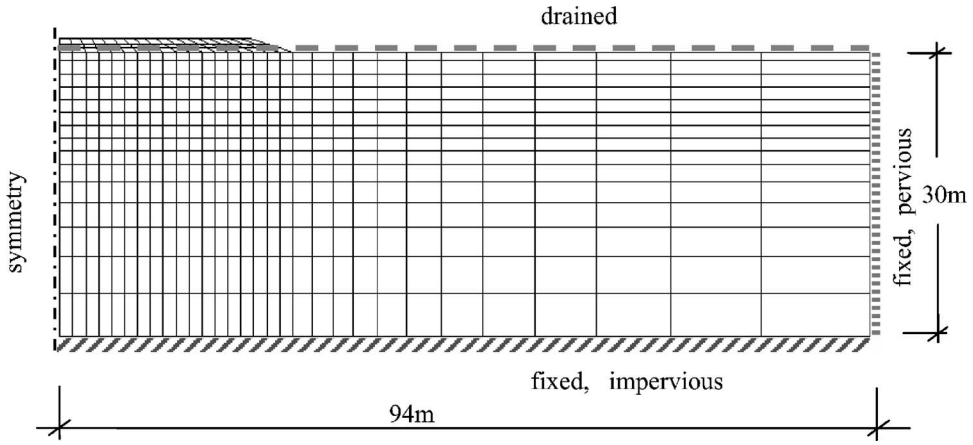

Fig. 3. Mesh for finite-element analysis

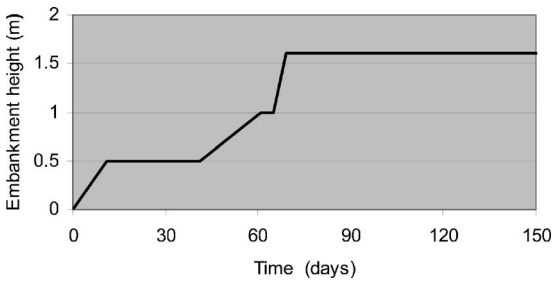

Fig. 4. Construction sequence of the Teven Road embankment

PC3-2 (5 m deep) and Point PC3-3 (7 m deep). Less data were collected from PC3-2, and after the peak, these data are not consistent with those from other points, and therefore, they are not used in the following assessment of results. The regional water table position is monitored with two remote piezometers. The average of these two readings has been used in calculating the excess pore pressures from the data.

The basic features of typical embankment behavior are reflected in the measured results. These include that excess pore pressure builds up in the soil foundation in response to the construction of the embankment. Dissipation starts immediately during the construction and continues afterwards. The measured pore pressures reach maximum values at the end of construction (Leroueil et al. 1978). The consolidation settlement develops in the foundation over time as the excess pore pressure dissipates and the load transfers gradually to the soil skeleton.

Numerical simulations were first performed using soil parameters given in Table 2, with an assumed permeability anisotropy ratio $r_k=k_h/k_v=2.0$ for all soil layers.

Due to inadequate data, assumed values have been used for the permeability in the indurated sand layer. A number of numerical tests have been performed with various values for the permeability in this sand layer (Layer 3). Here, the numerical results obtained with permeability coefficients of $k_{3v}=1.0\times10^{-5}$, 1.0×10^{-6}, and 1.0×10^{-7} m/s for the sand layer are considered (here and in the following, the subscript number for a soil parameter refers to soil layer with respect to Table 2). Comparison of predicted settlements with the measurements at Points A, B, C, and D is presented in Fig. 5. It can be seen that the early settlements are strongly influenced by the assumed permeability of the sand layer (though the total settlement is indifferent to the chosen value, as expected). With $k_{3v}=1.0\times10^{-6}$ m/s, numerical predictions of the settlements under the embankment (Points A and B) coincide very well with the measured results. The trend in the settlement curves shows a significant alteration at a time of around 60–70 days, which is found to be consistent with the time that the effective stress reaches the preconsolidation pressure in the upper clay layers. In response to this, an obvious heave is predicted at, and just beyond, the toe of the embankment. This heave is, compared with the measured results, slightly overestimated.

Numerically predicted excess pore pressures are presented in Fig. 6 in a comparison with the measured data. The predicted pore pressures reach maximum values at the end of embankment construction, and this is in general agreement with the measured data.

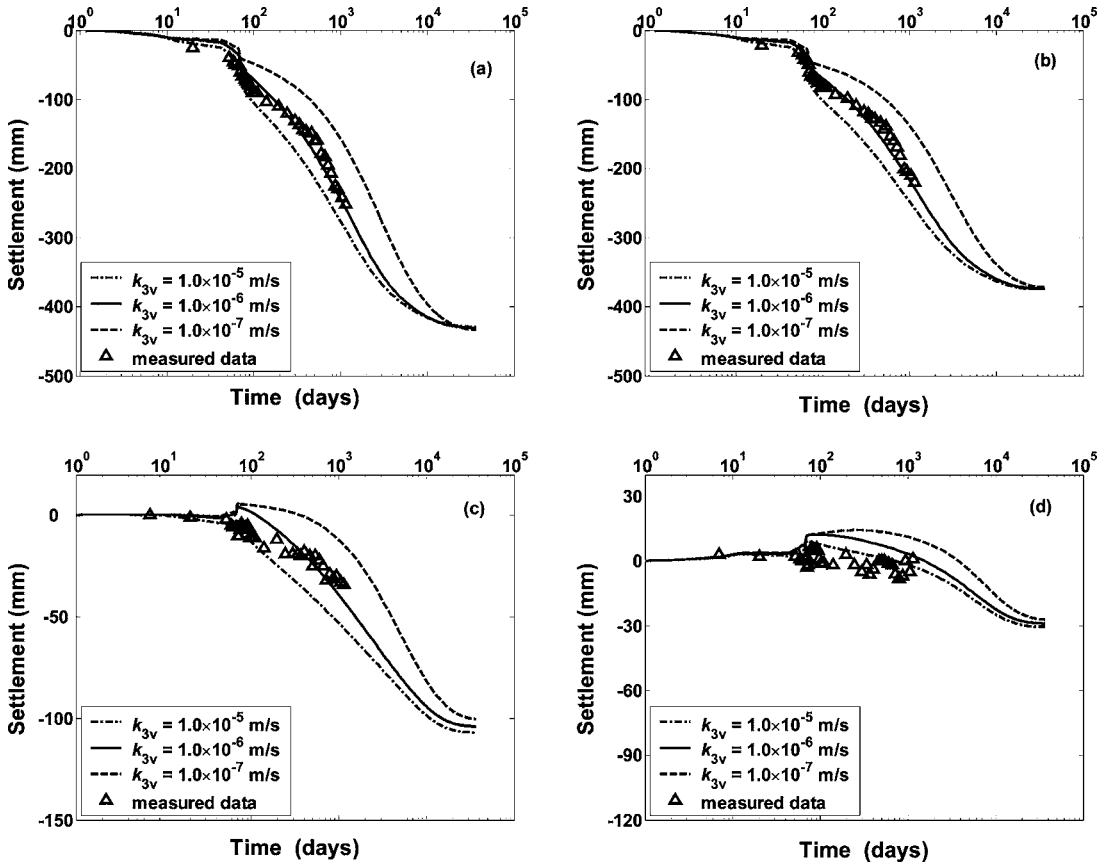

Fig. 5. Ground surface settlement obtained numerically for different sand permeabilities in comparison with the measurement at: (a) the center; (b) 15 m from the center; (c) the toe; and (d) 7 m outside the toe

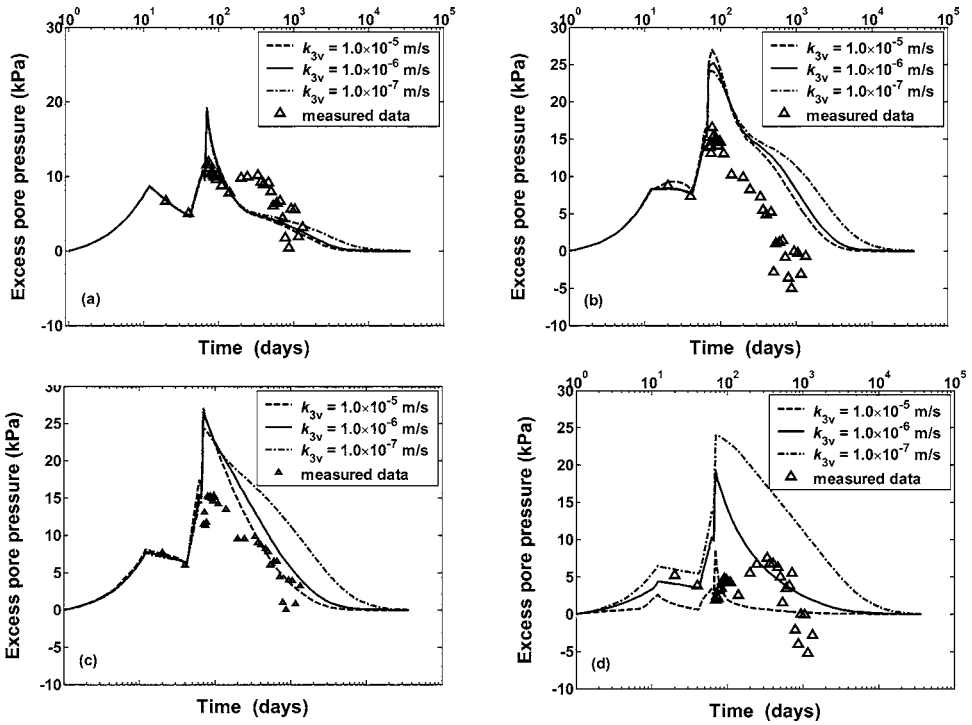

Fig. 6. Pore pressure from numerical prediction for different sand permeabilities in comparison with measured data under the embankment at Points (a) PC2-1; (b) PC2-2; (c) PC3-3; and (d) PC2-4

After the peak, the predicted pore pressures decrease consistently, approaching their initial values, as expected. The predicted dissipation rate in the sand and in the clay adjacent to the sand layer increases markedly as the sand permeability is increased. The predicted times for the excess pore pressure to be substantially dissipated in the upper soft clay layer (Layer 2) are about 13, 20, and 50 years, respectively, for values assumed for the hydraulic conductivity of the sand layer. Also, the magnitude of the predicted maximum excess pore pressure decreases as the sand permeability increases. In particular, the maximum excess pore pressure in the sand layer reduces significantly from 23.9 to 18.6, and 8.6 kPa as k_{3v} varies from 2.0×10^{-7} to 1.0×10^{-6} and 2.0×10^{-5} m/s.

Due to the nature of instrumentation, the quality of the data from pore pressure measurement is not as high as those measured for settlement. The measured data show some inconsistent variations over time and the excess pore pressures even become negative at some points. In particular, the excess pore pressure at PC2-4 (which is located in the sand layer) shows a second peak, occurring after the end of embankment construction. This variation of pore pressure in the sand layer may be explained as a result of a distant environmental influence on the confined sand layer. Consistent with the expectation of a higher hydraulic conductivity with respect to other layers, the sand layer can be more sensitive to the remote environment and the pore pressure may respond to remote changes, such as in the water level in the adjacent river. Despite these unexpected values, the peak excess pore pressure measurements at the end of embankment construction are considered acceptable, having values of 13.4, 16.6, 15.3, and 6.5 kPa, at PC2-1, PC2-2, PC3-3, and PC2-4, respectively. Their numerically predicted counterparts (for $k_{3v}=1.0\times10^{-6}$ m/s) are, respectively, 19.2, 25.2, 26.1, and 18.6 kPa, which are consistently greater than the measured data. A similar overestimation of maximum excess pore pressures has also been obtained from numerical modeling using the "in-house" finite-element program SNAC (Sheng 2003). The possible cause of this quantitative discrepancy between the predicted and the measured excess pore is discussed as follows.

The possibility of underestimation of soil permeability, which may affect the numerical prediction of pore pressure, is considered by systematically changing the hydraulic conductivity in the upper soft clay layer (Layer 2) in numerical modeling. Fig. 7 shows the variation of excess pore pressure and settlement of the ground surface under the embankment as the hydraulic conductivity k_{2v} for Layer 2 is increased to three and ten times its best-estimated value listed in Table 2 while the ratio $k_{2h}/k_{2v}=2$ is retained. It can be seen that a higher permeability corresponds to a lower excess pore pressure and a higher settlement rate. Corresponding to the change in hydraulic conductivity in k_{2v}, the maximum excess pore pressures vary from 25.2 to 20.5 and 17.3 kPa at PC2-2 (located in Layer 2). With $k_{2v}=10k_{2ve}$, the predicted excess pore pressure at PC2-2 matches the measured data. However, while an improvement in the agreement between the predicted and measured excess pore pressures is achieved for higher clay permeability, the corresponding predicted settlements deviate significantly from the measured data [Figs. 7(c and d)]. It can also be seen that the change of hydraulic conductivity in Layer 2 does not have much influence on the excess pore pressure at Point PC2-4 (located in the sand layer). This may be due to the sand layer having a much higher permeability.

Inadequate characterization of the anisotropy in the permeability may also affect the predicted peak excess pore pressure. This effect is examined by setting the permeability anisotropy ratio $r_k=1.0$, 2.0, 4.0, and 10.0, respectively, for all subsoil layers. Numerical results show that the peak values of the excess pore pressure in the soft clay layer change only slightly as the horizontal hydraulic conductivity increases, while the postpeak dissipation rate is obviously increased [Figs. 8(a and b)]. Similarly,

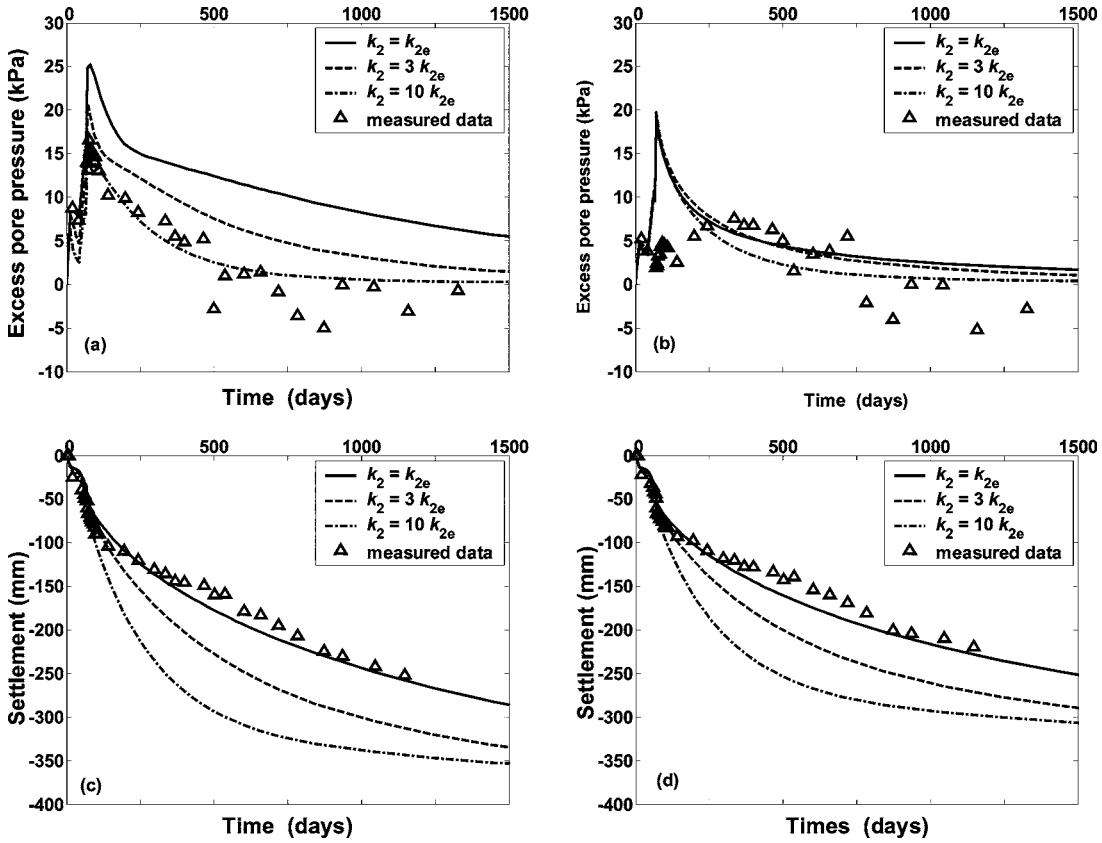

Fig. 7. Excess pore pressure at (a) PC2-2 and (b) PC2-4 and settlement at (c) center and (d) 15 m from the center, in response to the variation of permeability in the upper soft clay layer

higher horizontal permeability corresponds to a higher gradient of the settlement curves, and leads to a deviation of numerical prediction from the measurement [Figs. 8(a and b)]. In fact, the measured settlement curves are generally well matched for an anisotropy ratio r_k=2.0 [see, also, Fig 13(a)].

The above numerical results show that the development of settlement, and excess pore pressure cannot be concurrently predicted in a satisfactory manner by modifying soil permeability. A number of factors may play roles in the discrepancy between prediction and measurement. One of these factors is the limitation of the constitutive model. We note that the MCC model used in the present study is only a simple elastoplastic model, which is not adequate to reproduce the very complicated behavior of real soils. Adachi et al. (1985) showed that MCC model overestimates pore pressure in normally consolidated clay under undrained triaxial conditions. The accuracy of the elastic volumetric response of the model is also limited. It tends to overestimate the contractive volume change for stress states falling inside the yield surface, and this may result in an overestimation of excess pore pressure in overconsolidated soil layers. Leroueil et al. (1978) also reported that the measured excess pore pressures in embankment foundations are somehow systematically lower than expected. They suggested that the coefficient of consolidation c_v may be significantly underestimated in overconsolidated clay. This, in turn, leads to a pronounced overestimation of excess pore pressure in the early stage of loading. Other factors that may lead to an overestimation of excess pore pressure include assumption of full saturation of soils above the ground water level, and neglect of the slight compressibility of the pore water, which may contain small amounts of air. It is noted that an underestimation of the overconsolidation ratio may also increase the predicted excess pore pressure, as will be shown numerically, later in this paper.

Settlement Predictions

To date, the settlements have been monitored for about 1,300 days, which comprises only a small fraction of the expected total settlement time. As the early settlements are well captured by the finite-element modeling, it is considered likely that the total primary consolidation settlement may be well predicted also. In the finite-element simulation, the foundation deforms concurrently with the development and dissipation of excess pore pressure as load increases. Therefore, initial deformation is combined with the primary compression. At the center of the embankment, this total primary settlement prediction reads 431 mm, which matches the estimation based on the soil mechanics method.

Effect of the Compressibility Parameter and Overconsolidation Ratio

We note that our finite-element model is able to approximate 2D deformation with coupling of the pore water flow with soil deformation, and so, it is expected to provide better predictions than the simple 1D approach. However, the reliability of numerical results is strongly influenced by the input parameters. Differences may exist between the laboratory conditions under which the soils are tested and the in situ state of the soils beneath the embankment, and so the estimated soil parameters may deviate from their

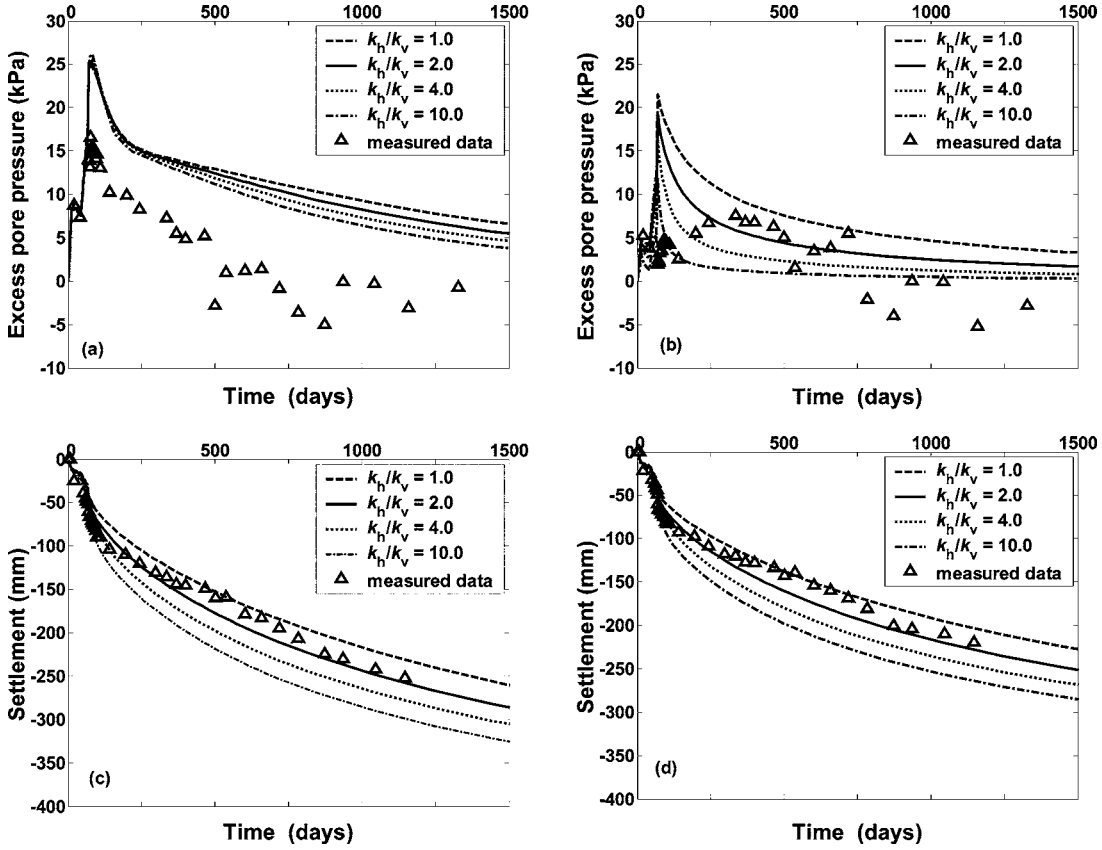

Fig. 8. Excess pore pressure at (a) PC2-2 and (b) PC2-4 and settlement at (c) center and (d) 15 m from the center, in response to the variation of permeability anisotropy in subsoil layers

actual values. It is, therefore, of interest to consider the sensitivity of the predicted settlements to the adapted soil parameters.

Among many factors, ground settlement is directly related to the soil compression parameters λ and κ, (as κ and λ determine soil compressibility in the elastic and plastic states, respectively), and to the overconsolidation ratio OCR (which affects the initial yield in soil). Numerical tests are performed to consider the sensitivity due to variations in the values of λ_2, κ_2, and OCR_2 for the upper soft clay layer. Fig. 9(a) shows the settlement response at the center of the embankment for λ_2/λ_{2e}=0.8, 0.9, 1.0, 1.1, and 1.2. Here, and in the following, the soil parameter with subscript e represents the (best-) estimate value listed in Table 2. It can be seen that the total settlement increases significantly as the value of λ_2 increases. However, the early stage settlement response is less sensitive to the variation of the compression parameter. This means that the measured settlement at the current time may be not sufficiently complete to enable a conclusive evaluation of the adopted values of the soil parameter λ, although the results do suggest that inaccuracy in λ may lead to a relative error as high as 13% in the prediction of the total settlement.

Some influence of the possible inaccuracy of κ_2 is observed in the early stage response, but this influence is generally insignifi-

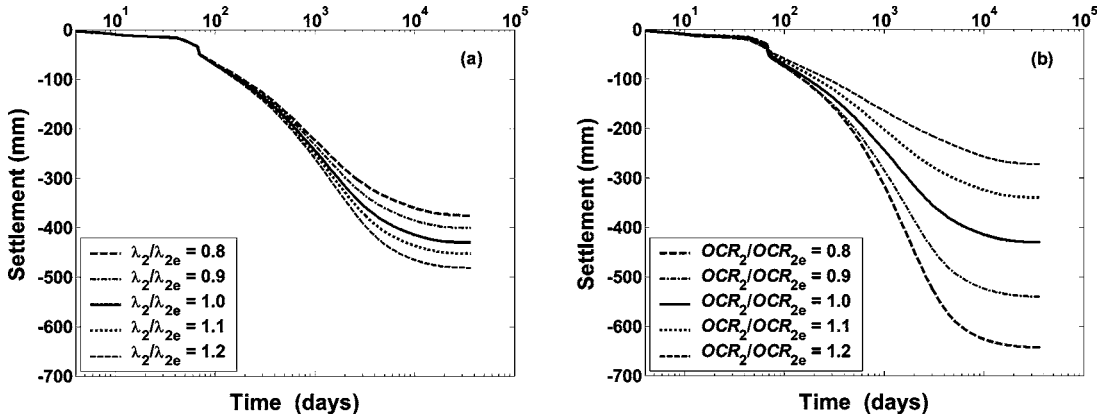

Fig. 9. Ground settlement at the center of the embankment, with respect to the variation of (a) soil compression parameter λ_2 and (b) overconsolidation ratio OCR_2 for the upper soft clay layer

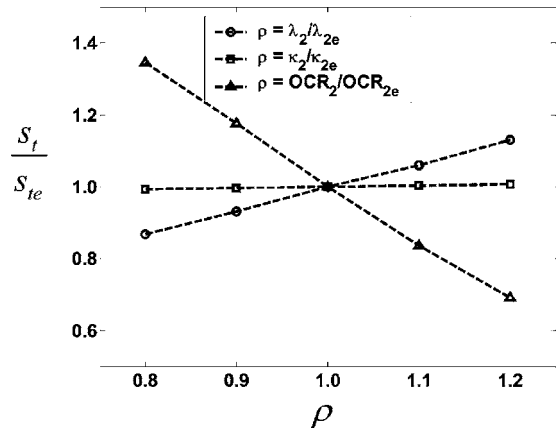

Fig. 10. Variation of settlement at the center of the embankment expressed by the ratio s_t/s_{te} with respect to $\rho=\lambda_2/\lambda_{2e}$, κ_2/κ_{2e}, and OCR_2/OCR_{2e} in the upper soft clay layer

cant. In contrast, the variation of OCR_2 has a much stronger influence on the predicted settlement, as can be seen in Fig. 9(b) showing the predicted settlement curves for $OCR_2/OCR_{2e}=0.8$, 0.9, 1.0, 1.1, and 1.2. Increase of the overconsolidation ratio results in a significant decrease in the predicted settlement. The relative sensitivity of predictions with respect to the variation of λ_2, κ_2, and OCR_{2e} is considered by comparing the total settlement at the center of the embankment, as shown in Fig. 10. It is clear that the total settlement is insensitive to the change of parameter κ, sensitive to the change of λ, and strongly sensitive to the OCR.

It was also found that λ has only a slight influence on the predicted excess pore pressure, whereas the excess pore pressure is strongly affected by the OCR. The peak excess pore pressure decreases significantly as the OCR increases (Fig. 11). Numerical results also show that the sensitivity of predicted excess pore pressures due to the soil parameter κ is almost negligible.

Compression of the Underlying Clay Layer

The lower clay layer (i.e., Soil Layer 4) lies at a depth from 11.5 to 30 m, and laboratory testing reveals that this clay layer is also normally consolidated with an overconsolidation ratio close to 1.0. As the embankment width exceeds 50 m, stress increments at this depth are expected to be significant, and so a large fraction of the overall ground settlement may be due to the compression of this deep, thick clay layer. In the 1D soil mechanics estimation presented earlier, compression of the lower clay layer contributes about 147 mm to the total consolidation settlement of 423 mm beneath the center of the embankment. In the finite-element modeling, the compression of the lower clay layer is reflected by the settlement of the sand layer. This estimated settlement of the sand layer beneath the center of the embankment is 139 mm.

The settlement at various depths beneath the embankment was to be measured in the field by vertical settlement profilers. Unfortunately, little data have been obtained from these instruments due to the buckling of the vertical profiler tubing early in the study. Consequently, the ability of the numerical model to accurately predict settlements in each of the soil layers cannot be readily assessed.

The numerical study has been extended to show the influence of possible errors in the related parameters to the settlement of the sand layer. It is found that the final settlement of the sand layer is almost unchanged for the elastic parameter of the sand layer κ_3 taking the values of $\kappa_3=0.1$, 1.0, and $10\kappa_{3e}$, respectively. In contrast, the variation in the plastic stiffness λ_4 of the underlying clay layer (Layer 4) significantly influences the predicted settlement of the sand layer, and consequently, the predicted settlement of the ground surface [Fig. 12(b)].

Lateral Displacement

Numerical predictions of the development of horizontal displacements under the toe of the embankment are presented in Fig. 13(a). The amount and direction of horizontal movement at the ground surface vary gradually in a manner that is consistent with the development of the surface settlement. The toe of the embankment is predicted to first move outwards and then backwards, which can be explained by bending of the ground surface due to the differential settlement over the full width of the embankment.

The location of the maximum horizontal displacement moves gradually from a depth of about 3 m to a depth of 6.5 m. Also, strong curvature is displayed in the upper part of the lateral deflection profiles, corresponding to thickness and position of the upper clay layer. For the Teven Road embankment, the presence of the sand layer has a notable effect on the shape of the lateral deflection curves. Due to the large difference between the stiff-

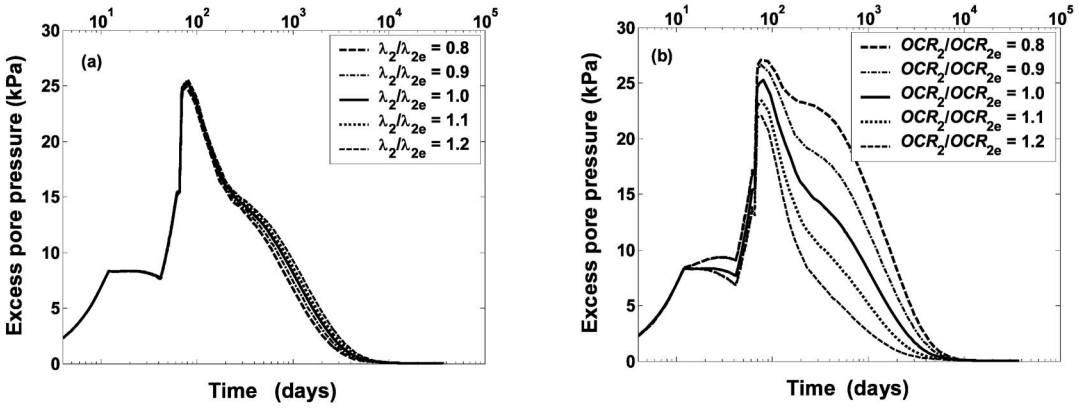

Fig. 11. Excess pore pressure at point at a depth of 5 m under the center line with respect to the variation of (a) λ and (b) OCR in the second subsoil layer

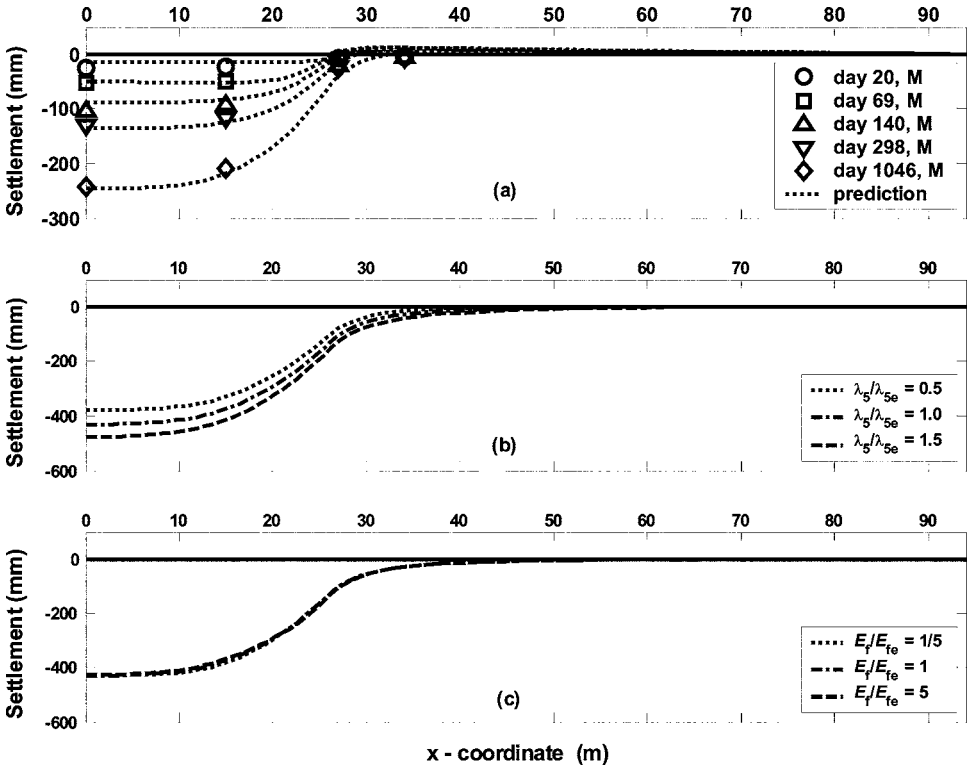

Fig. 12. Settlement of the ground surface: (a) predicted progressive settlement against the measured data; (b) variation of final settlement in response to the change of λ_4 for the lower soft clay layer; and (c) variation of final settlement in response to the change of the elastic modulus of the embankment fill

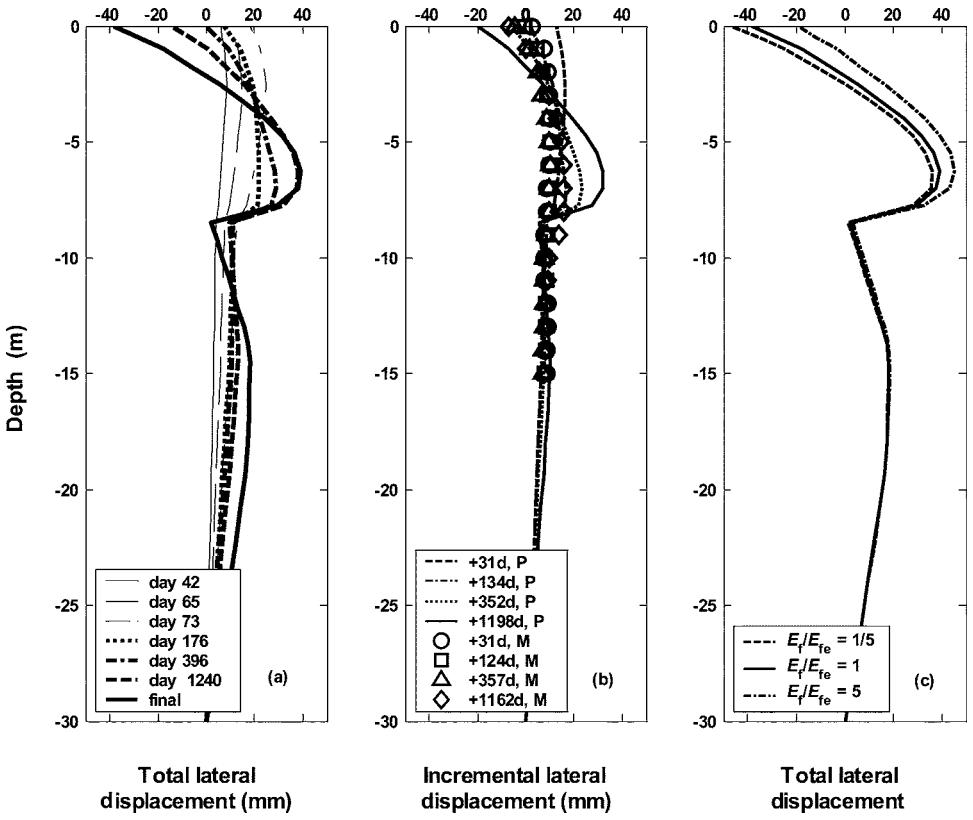

Fig. 13. Lateral displacements: (a) predicted total lateral displacements; (b) measured (*M*) and predicted (*P*) lateral displacements since Day 42; and (c) predicted final lateral displacements in response to different values for the elastic modulus of the embankment fill

ness of the sand and soft clay layers, a sharp kink develops in the deflection curves at the upper clay/sand interface, and the horizontal displacement in the lower clay layer seems somehow restricted by the sand layer. In effect, it is considered that the model predicts that the clay between the embankment fill and the sand layer is being squeezed from between these layers.

Verification of the predicted lateral soil deflections can be attempted by comparison with the measured data obtained from the horizontal displacement profiler installed under the toe of the embankment. However, since the first reading was taken 42 days after the start of construction, data for the first 42 days of lateral soil deformation do not exist. Comparison between numerical prediction and the measurement could thus only be made by assuming that the 42 day readings were the initial readings, and by considering the incremental change in the horizontal displacement with respect to the Day 42 data, as shown in Fig. 13(b). It can be seen that while there is general agreement, numerical predictions tend to overestimate the (incremental) horizontal displacement. This is consistent with the observations of many embankment studies (e.g., Poulos 1972; Rowe et al. 1995). Poulos noted that there are a number of possible reasons which may lead to discrepancies between calculated and measured results, including difficulty of estimating Poisson's ratio, anisotropy of the soil, and nonlinear stress–strain behavior of soil. In the present numerical study, the predicted lateral displacement can be improved by adopting a smaller Poisson's ratio ($\mu_1/\mu_{1e}=\mu_2/\mu_{2e}=1/3$). Although the reduced Poisson's ratio values (around 0.1) are low for clay soils, they do produce an improvement in the predicted lateral displacements, without significantly affecting the predicted vertical settlements. With respect to Eq. (5), this result can be explained as a consequence of increase of the shear modulus for the upper clay layers.

Intuitively, the embankment stiffness may have some influence on the lateral displacement of the underlying soil. The effect is examined by adapting different values of the elastic modulus for the fill in calculations. For $E_f/E_{fe}=1/5$, 1, and 5, the corresponding settlements of the ground surface are shown in Fig. 12(c), and the corresponding lateral displacements are presented in Fig. 13(c). It can be seen that change of the embankment stiffness affects mainly the lateral displacement near the toe of the embankment. The maximum horizontal displacement under the toe takes place at the same depth, while the value varies from 35.8 to 38.9 and 45.1 mm for $E_f/E_{fe}=1$, 1/5, and 5, respectively. The predicted ground settlement is insensitive to the stiffness of the embankment fill.

Conclusion

The consolidation behavior of an instrumented embankment on a soft soil foundation has been studied numerically using a coupled, nonlinear, finite-element analysis. Early stage numerical predictions have been compared with the measured field data. The effects of some key parameters on the predicted embankment performance have been examined by a parametric study.

Overall, good agreement with settlements has been demonstrated using the Modified Cam Clay model for clay layers. In particular, good agreement in magnitude for time-dependent vertical settlements has been obtained for the embankment. The final primary settlement is in good agreement with the prediction of 1D consolidation analysis. The lower clay layer can contribute a significant fraction to the total ground settlement, which is mainly controlled by the compressibility and thickness of this clay layer. The stiffness of the sand layer has little influence on the settlement predictions. The peak pore pressures are strongly influenced by the hydraulic conductivity. Among the many parameters used in the analysis, the plastic compressibility and the overconsolidation ratio have the strongest influence on the predicted settlement, while the latter also has a significant influence on predicted excess pore pressures. Predictions are relatively insensitive to the values of elastic compressibility that are adapted.

The present numerical model tends to overestimate the peak pore pressure systematically. Also, the horizontal displacement in the foundation is slightly overestimated. This can be partly improved by using a more advanced constitutive model and applying further sampling and laboratory testing for determination of relevant soil parameters. Modeling of unsaturated soil and effects of natural soil structures may also be helpful. Equally important is research into the reliable correlation between laboratory and field data and improvement of field instrumentation.

References

Adachi, T., Mimura, M., and Oka, F. (1985). "Descriptive accuracy of several existing constitutive models for normally consolidated clays." *Numerical methods in geomechanics Nagoya 1985*, T. Kawamoto and Y. Ichikawa, eds., Balkema, Rotterdam, The Netherlands, 259–266.

Al-Tabbaa, A., and Wood, D. M. (1987). "Some measurements of the permeability of kaolin." *Geotechnique*, 37(4), 499–503.

Biot, M. A. (1941). "General theory of three-dimensional consolidation." *J. Appl. Phys.*, 12, 155–164.

Bishop, D. (2004). "A proposed geological model and geotechnical properties of a NSW estuarine valley: A case study." *Proc., 9th ANZ conference on geomechanics*, G. Farquhar, P. Kelsey, J. Marsh, and D. Fellows, eds., New Zealand Geotechnical Society, Auckland, New Zealand, 261–267.

Bjerrum, L. (1967). "Engineering geology of Norwegian normally consolidated marine clays as related to settlements of buildings. 17th Rankine Lecture." *Geotechnique*, 17(2), 81–118.

Chandler, R. J., Leroueil, S., and Trenter, N. A. (1990). "Measurements of the permeability of London clay using a self-boring permeameter." *Geotechnique*, 40(1), 113–124.

Das, B. M. (1990). *Principles of foundation engineering*, PWS-KENT, Boston.

Desai, C. S. (2000). *Mechanics of materials and interfaces, the disturbed state concept*, Chap. 7, CSC, Boca Raton, Fla.

Gens, A., and Potts, D. M. (1988). "Critical state models in computational geomechanics." *Eng. Comput.*, 5(3), 178–197.

Gudehus, G. (1996). "A comprehensive constitutive equation for granular materials." *Soils Found.*, 36(1), 1–12.

Hibbitt, Karlsson, & Sorensen, Inc. (HKS). (2001). *ABAQUS/Standard user's manual, version 6.2*, HKS, Providence, R.I..

Leroueil, S., Tavenas, F., Trak, B., La Rochelle, P., and Roy, M. (1978). "Construction pore pressures in clay foundation under embankment. Part I: The Saint-Alban test fill. Part II: Generalized behavior." *Can. Geotech. J.*, 15(1), 54–82.

Leroueil, S., Tavenas, F., Bergeon, L., and La Rochelle, P. (1990). "Permeability anisotropy of natural clyss as a function of strain." *Can. Geotech. J.*, 27(5), 568–579.

Lo, K. Y., Bozozuk, M., and Law, K. T. (1976). "Settlement analysis of the Gloucester test fill." *Can. Geotech. J.*, 13(4), 339–354.

Lunne, T., Robertson, P. K., and Powell, J. J. M. (1997). *Cone penetration in geotechnical practice*, Blackie Academic & Professional, London.

Mesri, G., and Godlewski, P. M. (1977). "Time- and stress-compressibility interrelationship." *J. Geotech. Engrg. Div.*, 103(5), 417–430.

Mesri, G., and Choi, Y. K. (1985). "Settlement analysis of embankments on soft clays." *J. Geotech. Engrg.*, 111(4), 441–464.

Olson, R. E. (1986). "State of the art: Consolidation testing." *Consolidation of soils: Testing and evaluation, special technical publication no. 892*, R. N. Young and F. C. Townsend, eds., ASTM, Philadelphia, 7–68.

Poulos, H. G. (1972). "Difficulties in prediction of horizontal deformations of foundations." *J. Soil Mech. and Found. Div.*, 98(8), 843–848.

Poulos, H. G., and Davis, E. H. (1974). *Elastic solutions for soil and rock mechanics*, Wiley, New York.

Robert Carr & Associates. (2000). "Report on site investigation and instrumentation for the Cumbalum and Teven Road trial embankments." *Rep. No. 336T*, Robert Carr & Associates, Pty. Ltd., Newcastle, U.K.

Roscoe, K. H., and Burland, J. B. (1968). "On the generalized stress-strain behavior of "wet" clay." *Engineering plasticity*, J. Heyman and F. A. Leckie, eds., Cambridge University Press, London, 535–609.

Rowe, R. K., Gnanendran, C. T., Landva, A. O., and Valsangkar, A. J. (1995). "Calculated and observed embankment over soft compressible soil." *Geotechnique*, 32(3), 512–534.

Sheng, D. (2003). "Finite-element analysis of a test embankment on soft clay." *Proc., 12th Asian Regional Conf. on Soil Mechanics and Geotechnical Engineering*, C. F. Leung, et al., eds., World Scientific, Singapore, 755–758.

Wathugala, G. W., and Desai, C. S. (1993). "Constitutive model for cyclic behavior of clay. I: Theory." *J. Geotech. Engrg.*, 119(4), 714–729.

Whittle, A. J., and Kavvadas, M. J. (1994). "Formulation of MIT-E3 constitutive model for overconsolidated clays." *J. Geotech. Engrg.*, 120, 173–198.

Wood, D. M. (1990). *Soil behavior and critical state soil mechanics*, Cambridge University Press, London.

Wroth, C. P. (1975). "In situ measurement of initial stresses and deformation characteristics." *Proc., Specialty Conf. on In Situ Measurement of Soil Properties*, Vol. 2, Raleigh, N.C., ASCE, Reston, Va., 181–230.